Journal of Materials Chemistry

www.rsc.org/materials

Volume 20 | Number 13 | 7 April 2010 | Pages 2481–2692

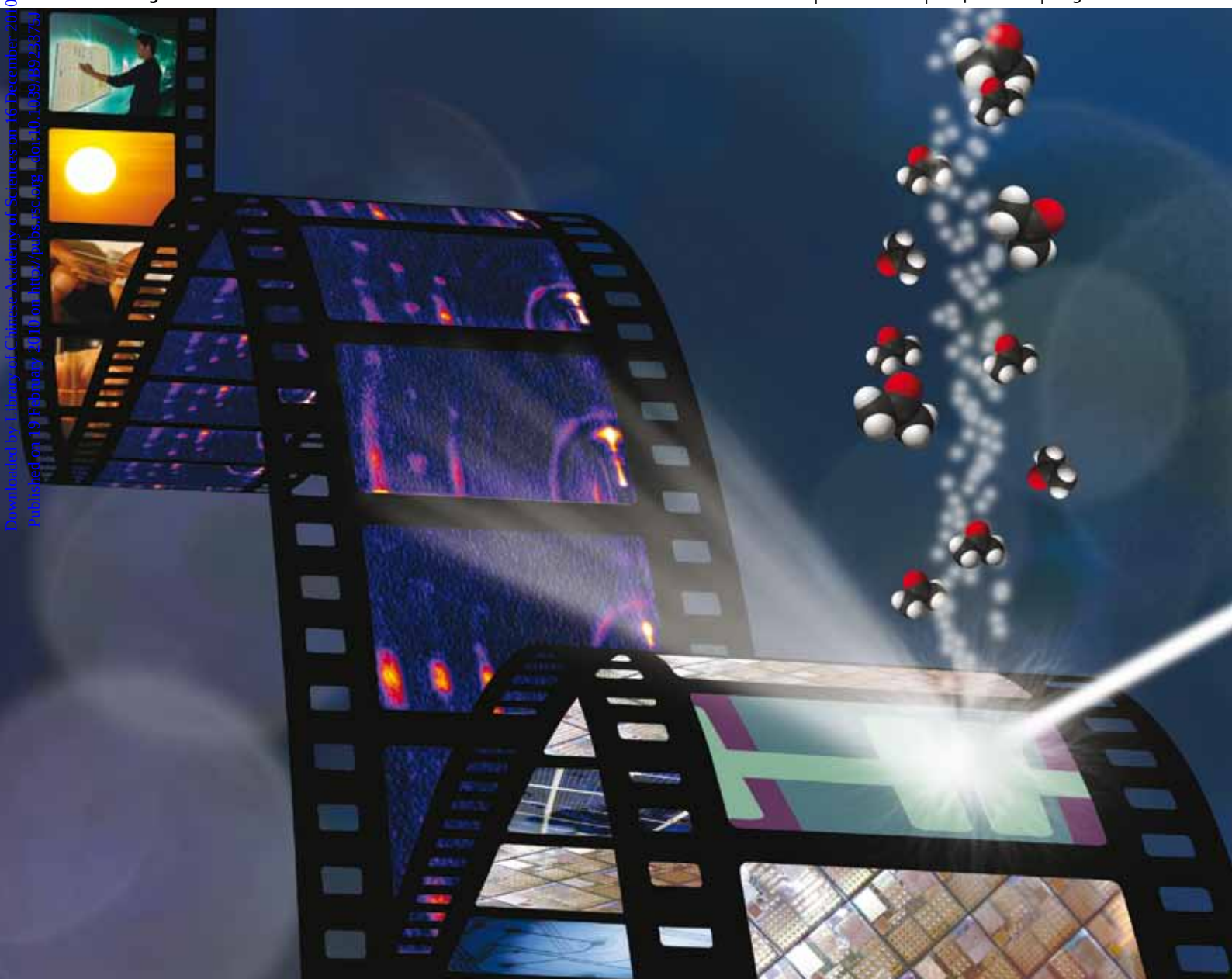

Interface Engineering of Organic and Molecular Electronics

ISSN 0959-9428

RSC Publishing

0959-9428(2010)20:13;1-R

Solvent vapor annealing of an insoluble molecular semiconductor†

Aram Amassian,*[a] Vladimir A. Pozdin,[b] Ruipeng Li,[a] Detlef-M. Smilgies[c] and George G. Malliaras*[b]

Received 6th November 2009, Accepted 15th January 2010
First published as an Advance Article on the web 19th February 2010
DOI: 10.1039/b923375j

Solvent vapor annealing has been proposed as a low-cost, highly versatile, and room-temperature alternative to thermal annealing of organic semiconductors and devices. In this article, we investigate the solvent vapor annealing process of a model insoluble molecular semiconductor thin film—pentacene on SiO_2 exposed to acetone vapor—using a combination of optical reflectance and two-dimensional grazing incidence X-ray diffraction measurements performed *in situ*, *during* processing. These measurements provide valuable and new insight into the solvent vapor annealing process; they demonstrate that solvent molecules interact mainly with the surface of the film to induce a solid–solid transition without noticeable swelling, dissolving or melting of the molecular material.

Introduction

Organic electronics (OE) is a very active field of research in large part because of the promise of low-cost and large-area processing and fabrication of organic thin film transistors (OTFTs) and photovoltaics (OPV) on flexible substrates.[1–5] The fabrication steps of organic semiconductors and their devices prepared *via* vacuum and solution routes typically involve post-processing steps designed to tailor the structure and electronic properties of key components to the requirements of the application.

In the case of most solution-processed organic semiconductors, post-processing most commonly implies thermal annealing as a means of promoting crystallization and grain growth for OTFTs, and as a means of influencing the nanoscale phase separation of bulk heterojunctions to better meet the efficiency requirements of OPV devices.[5–11] While thermal annealing is attractive and highly popular due to its simplicity and efficacy, it has inherent limitations which can be especially acute in the case of organic semiconductors.[12–14] Molecular building blocks tend to be less strongly bound than their inorganic counterparts, which can cause important loss of material and reorganization *via* desorption,[15] and dewetting,[16–18] respectively; both phenomena can be observed near room temperature, but become far worse when samples are heated.[19] The thermal load applied during processing of subsequent layers of a device can also have unintended consequences on the electronic structure of buried thin films and interfaces by inducing undesired phase transformation and segregation, grain growth, interdiffusion, or cracking.[8,20,21] Heating also promotes oxidation and chemical degradation of molecular building blocks,[22,23] thus causing significant decay in device performance.[24,25] Annealing can be performed under inert atmosphere or in vacuum to reduce chemical degradation; but, this does not prevent structural changes or dewetting.[17,26]

Solvent vapor annealing has recently emerged as an intriguing alternative to thermal annealing, because of its ability to operate at room temperature. Molecules from the solvent vapor adsorb on and interact with exposed surfaces and can, in principle, be non-interacting or orthogonal with critical organic or inorganic components of the device.[27–30] Solvent vapors therefore provide hitherto unexplored opportunities to control material characteristics in a targeted manner with unprecedented versatility, while reducing the thermal load applied to OE devices.

Solvent vapor annealing of popular material systems in OE, such as pentacene,[31,32] blends of P3HT:PCBM,[5,8,33] and others[34,35] have been reported with demonstrated benefits to the performance of devices, wherever intended. However, the complexities inherent to the interaction of solvent molecules with molecular building blocks of the semiconductor thin films and the large gap between our current understanding and mastery of thermal and solvent annealing processes make it challenging to develop and scale up processing strategies tailored to target specific materials and device components without first understanding the effects of solvent vapor annealing on molecular thin films.

In this article, we use a combination of two-dimensional grazing incidence wide angle X-ray scattering (GIWAXS) and time-resolved optical reflectometry to monitor the solvent vapor annealing of a model insoluble molecular semiconductor thin film—pentacene on SiO_2—as it is exposed to acetone vapor. Pentacene is known to undergo a phase transformation from the "thin film" to the bulk phase when exposed to certain solvent vapors despite its well-known solvent resistivity.[31] This work reveals that solvent molecules interact with the thin film through its surface, where they tend to remain throughout the solvent annealing process and gradually transform the "thin film" phase to the bulk phase. The molecular thin film does not dissolve or melt throughout the process, indicating most likely a solvent-induced solid–solid phase transformation.

[a]*Materials Science and Engineering, Division of Physical Sciences and Engineering, King Abdullah University of Science and Technology, Thuwal, Kingdom of Saudi Arabia. E-mail: aram.amassian@kaust.edu.sa; Tel: +966(0)544700079*
[b]*Materials Science and Engineering, Cornell University, Ithaca, NY, 14853, USA. E-mail: ggm1@cornell.edu*
[c]*Cornell High Energy Synchrotron Source, Cornell University, Ithaca, NY, 14853, USA; Tel: +1 607 255 0917*

† This paper is part of a themed issue of *Journal of Materials Chemistry* on Interface engineering of organic and molecular electronics, guest edited by Alex Jen.

Results

The experimental apparatus used to perform and monitor solvent vapor annealing is presented in Fig. 1.[36,37] The cell consists of an air-tight aluminium enclosure with two Kapton windows, a valved inlet for liquids, gas inlets and outlets, as well as gas flow controllers located upstream and downstream of the chamber; the latter was used to verify the air-tightness of the cell. The sample, consisting of a vacuum-sublimated thin film of pentacene (~33 nm) deposited on monocrystalline Si with a 361.2 nm thick thermal oxide layer, is placed on a holder located in the center of the cell. To generate solvent vapor, we use a syringe to inject a few millilitres of solvent into a reservoir located at the base of the cell. The buildup of solvent vapor pressure is regulated by controlling the flow rate of He gas through the cell.

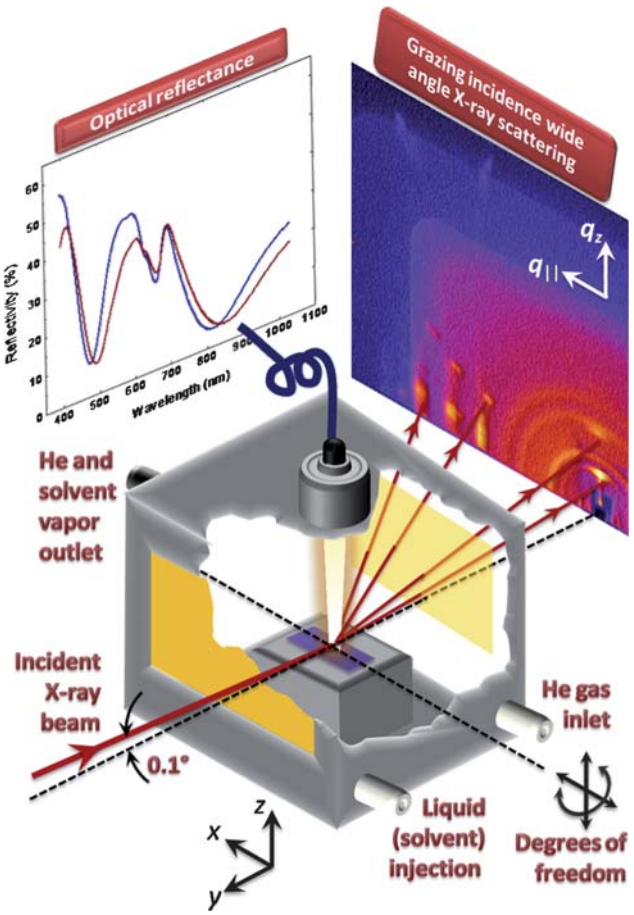

Fig. 1 Schematic representation of the solvent vapor annealing cell. The airtight cell is fabricated from aluminium and is mounted on a Huber stage. The solvent vapor annealing is initiated by injecting acetone from a syringe connected to the solvent inlet, while solvent vapor buildup is regulated *via* He gas flow through the cell. Another flow controller is placed downstream to verify the air-tightness of the cell by measuring the outgoing flow rate. A GIWAXS image is shown for a film that has undergone phase transformation to the bulk phase *via* solvent vapor annealing. Reflectance spectra taken before (blue) and during (red) solvent vapor annealing are shown as examples of measurements indicating spectral red-shift in the presence of solvent vapor molecules on the sample.

Optical reflectometry measurements (FilMetrics F30 spectrometer; 400 nm < λ < 1100 nm) were performed *in situ* and in real time during solvent vapor annealing to detect variations in the optical response of the sample in case its thickness or optical properties change. The reflectance spectra of the sample [*cf.* Fig. 1] exhibit interference maxima and minima, whose spectral positions depend upon the combined optical thicknesses, OT, of the SiO_2 and pentacene layers, since the Si wafer behaves—optically—as a semi-infinite medium. Optical thickness at a given λ is defined as the product of physical thickness and refractive index. If the optical thickness changes due to solvent uptake, then the positions of the maxima and minima (λ_{min}) will shift accordingly by $\Delta\lambda_{min}$; this can be monitored quantitatively to provide real-time information about the amount of solvent adsorption/condensation at the surface or into the film (see below).[36]

The structure of pentacene was monitored by GIWAXS. A monochromatic X-ray beam (10 keV; D-line; Cornell High Energy Synchrotron Source) is incident through the Kapton window at 0.1° relative to the sample surface, scatters off the sample, and the scattered signal is collected downstream on a 1024 × 1024 pixel CCD camera at a rate of ~0.1 Hz. A thin Al attenuator was used to reduce the intensity of the out-of-plane Bragg sheets to within the dynamic range of the detector; this made it possible to acquire both in-plane and out-of-plane features without compromising the signal-to-noise ratio of the weaker Bragg peaks.

In Fig. 2(a), we plot the time evolutions of He flow and the corresponding spectral shift, $\Delta\lambda_{min}$, for the minimum located initially at λ_{min} ~475 nm. He flow is initially set to ~130 sccm and allowed to evacuate the air from the cell 20 min prior to beginning the experiment. Solvent is injected into the cell ~2 min after start of data acquisition (t = 0). The elevated flow rate of He prevents the solvent vapor from building up uncontrollably and controls the onset of solvent vapor annealing. A small shift ($\Delta\lambda_{min}$ ~1–2 nm) detected several minutes after solvent injection in conditions of maximum He flow indicates that trace amounts of acetone adsorb on the surface of the sample. He flow is reduced first to 80 sccm (t = 600 s) with little additional change of $\Delta\lambda_{min}$, then to zero (t = 900 s) to achieve maximum vapor pressure. This leads to substantial red-shift, which proceeds rapidly at first ($\Delta\lambda_{min}$ changes by as much as ~16 nm in approximately 1 min), then converges asymptotically toward $\Delta\lambda_{min}$ ~19 nm. After ~40 min in maximum solvent vapor pressure at room temperature, He flow was raised to 130 sccm and $\Delta\lambda_{min}$ returned immediately to ~4 nm and decreased gradually to ~2–3 nm. This indicates that most of the solvent can be removed from the surface almost immediately, while some residual solvent remains trapped by the pentacene thin film.

The amount of solvent uptake can be estimated quantitatively by fitting a layered optical model of the sample to the measured reflectance spectra. In the simplest case, we can model the solvent as a simple liquid layer formed on the surface of pentacene [acetone(liquid)/pentacene/SiO_2/c-Si]. Simulations performed using the WVASE32 software found that as a general rule a change of λ_{min} by ±1 nm is equivalent to a change of *ca.* ±1.6 nm in equivalent thickness of the acetone layer. The thickness of the acetone layer can be determined unambiguously by fitting the layered model (above) to the reflectance spectra

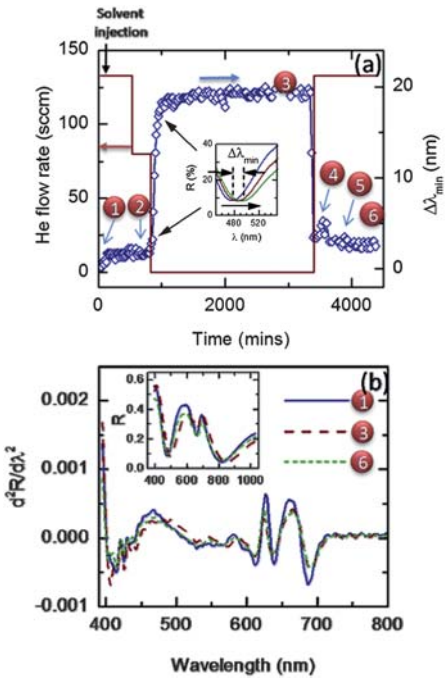

Fig. 2 Optical reflectance of pentacene thin films in response to changing flow rate of He. (a) Evolution of the flow rate of He through the cell during a typical solvent annealing experiment, along with the corresponding spectral shift, $\Delta\lambda_{min}$, of the reflectance (interference) minimum located at λ_{min} = 474 nm [see inset of (a)]. The numerical markers (1–6) correspond to key milestones of solvent annealing; they are referred to in all subsequent figures. (b) Second order derivative of reflectance with respect to wavelength as calculated from reflectance spectra [shown in inset of (b)] which were obtained before (1), during (3), and after (6) solvent vapor annealing.

presented in the inset of Fig. 2(b). In fact the acetone layer thickness is the only unknown in the fit, because the optical properties of all materials (acetone, pentacene,[38] SiO_2, and c-Si) are known from literature, while the thickness of the SiO_2 (361.2 nm) and pentacene (33 nm) layers are known from independent reflectance measurements performed on the same sample before and following deposition of the pentacene thin film.

The analysis of solvent uptake reveals that an amount of acetone equivalent to a ~2.5 nm thick liquid layer is adsorbed on the surface of pentacene when the solvent is initially injected [see marker (2) in Fig. 2(a)]. At maximum vapor pressure of acetone, the amount of acetone increases to ~30 nm [see marker (3) in Fig. 2(a)]. This amounts to a surface coverage of $\sim 2.5 \times 10^{16}$ acetone molecules cm^{-2}, or as many as ~3 acetone molecules for every pentacene molecule present on the substrate.

To confirm that these molecules are indeed located on the surface of the film, rather than incorporated into unit cells of the crystallites or at the semiconductor–dielectric interface, it is necessary to evaluate the film's crystallinity and the integrity of its lamellar texture as the solvent is taken up by the film. Optical reflectance measurements of the polycrystalline pentacene thin film can indirectly tell us if the polycrystalline film loses its long-range order throughout the process. Schreiber and coworkers showed the optical properties and absorption spectra of pentacene thin films are closely linked to the environment of pentacene molecules, *i.e.*, monomers in a solvent *vs.* in a crystallite.[38,39] The spectral features associated to the electronic transitions of the pentacene thin film can therefore tell us if acetone molecules cause widespread disorder throughout the film, as would be expected if several acetone molecules were to incorporate in each unit cell of pentacene lattice and swell the film.

In the range of interest of film thickness, the interference oscillations of the reflectance constitute a slowly varying signal, while the spectral features associated to the vibronic peaks of the polycrystalline semiconductor are comparatively sharp [*cf.* inset of Fig. 2(b)]. Hence, we apply a method from Auger spectroscopy, to use the second order derivative of the reflectance curve to highlight the sharp spectral features associated to the electronic structure of pentacene. Comparison between the spectra of pentacene taken before (1), during (3) and well after (6) solvent vapor annealing [*cf.* Fig. 2(b)] shows only slight variations in the shape and position of these spectral features [see plots (1) and (3)]. More importantly, these features do not disappear during solvent annealing; in fact, the spectra undergo irreversible changes upon exposure to solvent [compare plots (3) and (6) to plot (1)], which indicates that the structure of the pentacene film changes without any evidence of reversibility, such as swelling or expansion of lattice parameters due to solvent uptake, followed by contraction due to solvent release. Further confirmation of these claims may be obtained directly from X-ray diffraction measurements.

GIWAXS measurements taken before (1), during (2–3), and after (4–6) exposure of the sample to the solvent vapor [*cf.* Fig. 3] offer a sampling of the structural evolution of the pentacene thin film at various stages of the solvent vapor annealing process. The images reveal a structural transition from the "thin film" (1 and 2) to the bulk (3–6) phase without a noticeable movement of peak positions, or decrease of peak intensities, indicating retention of long-range order and unit cell parameters throughout the process. Retention of long-range order during solvent vapor annealing suggests that solvent molecules do not dissolve the pentacene crystallites; instead, solvent molecules appear to remain near the film surface and grain boundaries, from where they modify its structure.

The GIWAXS snap shots capture a number of useful features, including the diffuse Bragg sheets—for which the Bragg condition is not met under grazing incidence conditions—and in-plane Bragg peaks along the {11*l*}, {20*l*}, and {21*l*} crystal truncation rods (CTRs).

In Fig. 4(a) and (b), we plotted the {11*l*} CTR and the azimuthal intensity profile of $(001)_{BS}$, respectively. In (1) and (2), the in-plane diffraction peaks are associated predominantly with the "thin film" phase of pentacene, but the bulk phase is already seen after solvent is injected in the cell [*cf.* B_1 and B_3 in (2); Fig. 4(a)] and the surface has taken up the equivalent of ~2–3 monolayers of acetone. As more acetone molecules condense on the surface (3), the "thin film" diffraction spots become weaker, while the bulk phase diffraction spots become more intense. This suggests that the solvent molecules are responsible for initiating a solid-to-solid transition from "thin film" to bulk phase.

To get further insight into the phase transformation, we have plotted in Fig. 5 the time-evolution of the integrated peak intensities of the selected "thin film" (TF_2) and bulk (B_3) diffraction peaks. We selected TF_2 and B_3, because they do not

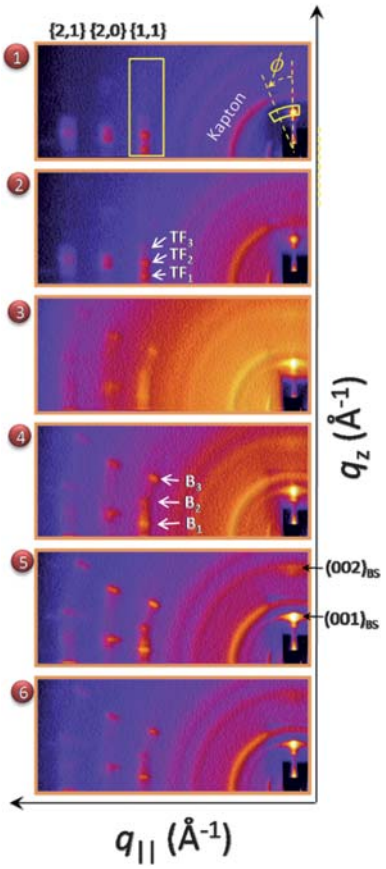

Fig. 3 GIWAXS snapshots taken before (1), during (2, 3) and after (4–6) solvent vapor annealing of pentacene. The (11*l*), (20*l*) and (21*l*) crystal truncation rods (CTR) and $(001)_{BS}$ are identified in (1). For future reference, we have labeled Bragg peaks with increasing q_z along the (11*l*) CTR as TF_1 (B_1), TF_2 (B_2), and TF_3 (B_3) for the "thin film" (bulk) phase. The rectangular box in (1) shows the region of integration (along $q_{||}$) used to calculate the line profile of the (11*l*) CTR [*cf.* Fig. 4(a)]. The azimuthal intensity profile of the Bragg sheet is calculated by integrating radially at each ϕ value along the box shown in (1). Notice the increased background intensity in (3) as a result of X-ray scattering from the solvent vapor molecules located in the path of the X-ray beam traveling through the cell.

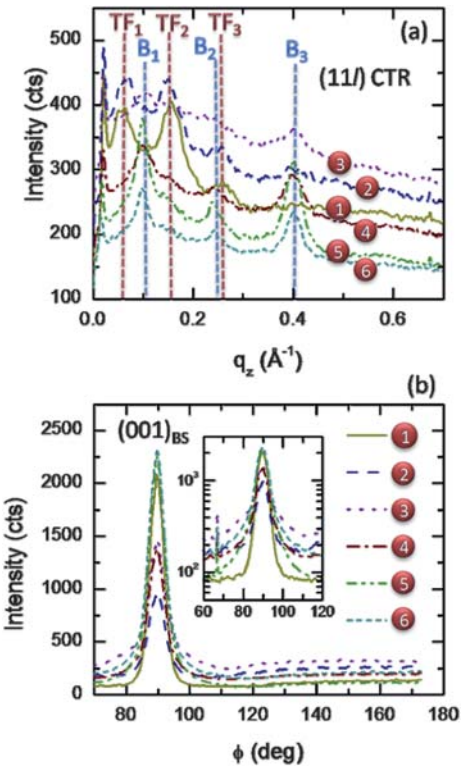

Fig. 4 Intensity profiles along the (a) (11*l*) CTR and (b) the (001) Bragg sheet calculated from GIWAXS snapshots presented in Fig. 3.

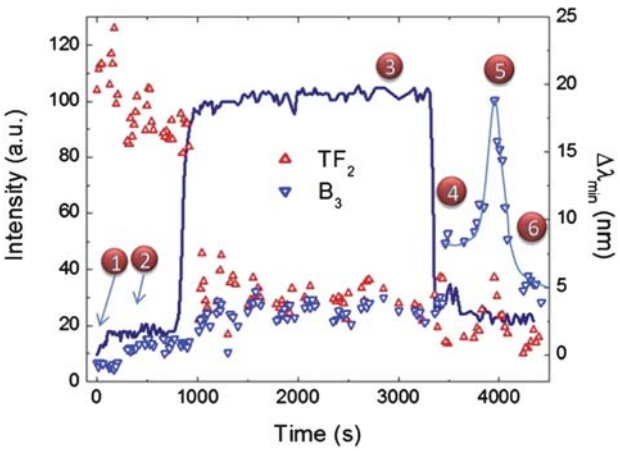

Fig. 5 Time-evolution of the integrated peak intensities of TF_2 and B_3 peaks associated to the "thin film" and bulk phases of pentacene. The wavelength shift, $\Delta\lambda_{min}$, is also shown for reference. As a guide to the eye, we have plotted a solid curve around the time when the unusual peaking behavior of B_3 occurs (4–6).

overlap with other peaks, thus simplifying the analysis. For reference, we also show $\Delta\lambda_{min}$ in the same plot. Fig. 5 reveals a close association between the amount of solvent adsorbed on the surface and the prevalence of the "thin film" and bulk phases. At this stage of the process, the extent of bulk phase formation is highly dependent upon the amount of solvent adsorbed on the surface, as indicated by the close association between the intensity of the B_3 peak and solvent uptake [*cf.* Fig. 5]. Even adsorption of a small amount of solvent vapor [as in (2)] initiates formation of the bulk phase. The bulk phase grows further when additional solvent vapor is provided to the film. This suggests that phase transformation is limited by supply of solvent molecules at or from the film surface. It also suggests that both the phase transformation and polymorphism of the thin film can be controlled by tuning the solvent vapor pressure in the cell.

Removal of solvent from the chamber leads to a further rise of the intensity of the B_3 peak, suggesting that the presence of the solvent introduced a level of disorder into the film. The (001) Bragg sheet becomes weaker and broader in angle during solvent annealing, as seen in (3–6) [*cf.* Fig. 4(b)]. The Bragg sheets strengthen, but do not recover the initial peak sharpness after the solvent is removed, indicating some irreversible degradation. The angular spread suggests that the lamellar structure of the film may be compromised during solvent annealing, most likely as a result of some local cracking and bending as crystallites undergo a substantial contraction (~6%) in the out-of-plane direction and a biaxial expansion (~2.5%) in the plane of the

substrate, as the surface of crystallites transform from "thin film" to bulk phase.[31,40]

A surprising phenomenon is observed in Fig. 5 several minutes after solvent vapor is evacuated from the cell and B_3 has plateaued for several minutes ($3400 < t < 3700$ s). An unusual peaking behavior occurs for B_3 [see marker (5) from $3700 < t < 4300$], characterized by a remarkable rise in the intensity of B_3 followed by a return to a weaker intensity. TF_2 also peaks, but to a much lesser extent than B_3. The increased intensity around the peaking behavior is also seen in GIWAXS images and CTR plots featured in Fig. 3 [see image (5)] and in Fig. 4 [see plot (5)], respectively. All diffraction spots and $(001)_{BS}$ become temporarily more intense even as the background signal is maintained. This behavior is unrelated to fluctuations of the intensity of the X-ray source, since all images were normalized to monitor count from an ion chamber (detector) placed in the X-ray beam path upstream of the cell. The monitor count decreases by no more than ~5% throughout the entire experiment. This effect is therefore material- and process-related, as we discuss below.

Discussion

In plotting the time-evolution of the intensity of TF_2 and B_3 diffraction peaks in Fig. 5 ($0 < t < 3000$ s), we note the absence of a one-to-one ratio between the rise of B_3 intensity and decrease of TF_2 intensity as the "thin film" phase transforms into the "bulk" phase. Such a simple 1 : 1 ratio may not be expected, because the structure factors of both peaks have to be taken into account. A quantitative comparison can therefore not be made if the structure factors are unknown.[41]

Microstructural differences between the "thin film" and bulk phases should also be taken into account. The "thin film" phase is formed on a very smooth template, *i.e.*, the surface of thermal SiO_2, whereas the bulk phase formation is initiated during solvent annealing from the rough and mounded surface of crystallites, as schematically illustrated in Fig. 6(a–c). For each monolayer of "thin film" phase that transforms into bulk phase, a coherent X-ray reflection is removed from the total intensity of the TF_2 peak. However, each layer of bulk phase that forms on the surface or the sides of adjacent crystallites with different dimensions and out-of-plane *d*-spacing may be slightly out-of-phase with bulk layers located on neighboring crystallites, because the underlying "thin film" phase monolayers possess different thickness and *d*-spacing. Consequently, formation of bulk phase monolayers at the surface may not contribute constructively to increasing the intensity of the B_3 peak, as would happen if all monolayers of the bulk phase were spaced by the same value.[42]

Furthermore, the bending, buckling or cracking that the pentacene film and crystallites undergo as a result of the ~6% contraction in the out-of-plane direction may be even more determining for the intensity of Bragg peaks. Formation of defects—as idealized in Fig. 6(c)—is partly due to the bulk phase growing from the rough surface of pentacene, rather than from

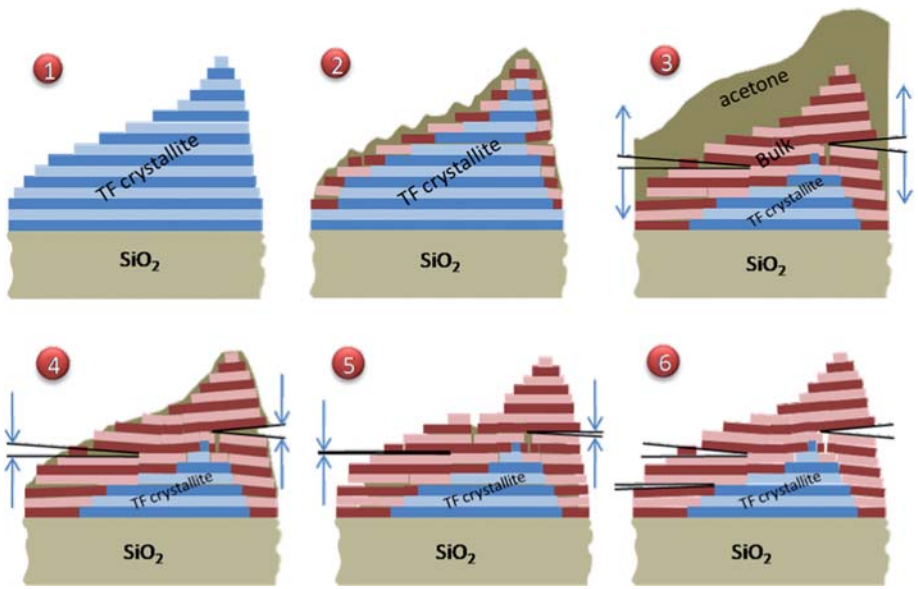

Fig. 6 Cartoons illustrating the gradual changes of a pentacene crystallite during solvent vapor annealing. Alternative light and dark lines are used to illustrate distinct monolayers of the "thin film" (dark and light blues) and bulk (dark and light reds) phases. Red lines are ~6% thinner than blue lines to account for the lattice compression in the out-of-plane direction [31]; the in-plane biaxial expansion (2.5%) is ignored for simplicity. (1) Pristine "thin film" crystallite grown on SiO_2, and forming a perfectly lamellar structure; (2) small amount of solvent adsorbed at the surface of pentacene leads to bulk phase formation in near-surface unit cells, thus forcing the red lines to bend slightly in order to remain attached to the crystallite; this can cause the edges of the crystallite to become slightly tilted with respect to the plane of the substrate and can lead to cracking near the surface of the film to accommodate the phase transformation. (3) As more solvent is made available, molecules penetrate into defects and cracks and facilitate phase transformation in deeper parts of the film, while also disturbing the lamellar quality of the affected regions. (4) The layer of acetone is easily evaporated when He flow increases, leaving behind residual acetone trapped in nanoscale cracks and pores formed in the surface and near grain boundaries. (5) As solvent evaporates from the pores and exposes the internal surfaces, we believe that the capillary pull attempts to reduce the total surface area of the system and brings the layers of the bulk phase into better alignment; this results in increased diffraction intensity and reduces the azimuthal spread of the Bragg sheets. (6) As the solvent leaves the pores, the material relaxes back into a less ordered state.

the smooth interface. The fact that the Bragg sheet remained broad even after the solvent vapor was evacuated indicates that the lamellar structure does not recover to its pre-annealing level [*cf.* Fig. 6(d)], in agreement with the hypothesis of a somewhat damaged film caused by solvent annealing.[34] The structure of pentacene shown in Fig. 6(c) may therefore explain the weak in-plane scattering by the thin film, as well as the texture of the lamellar structure revealed by the azimuthal spread of (001) Bragg sheet. The transient increase in X-ray diffraction intensity shown in Fig. 3–5 [see marker (5)] may be explained by evoking the same microstructural model of phase change as above. *A priori*, the dramatic increase of B_3 intensity suggests that the film becomes more crystalline temporarily, then reverts to a less crystalline state. However, this scenario is highly unlikely and thermodynamically inconsistent. Instead, we tentatively associate this behavior to a kinetic process, whereby capillary forces as a byproduct of solvent removal from cracks induce transient ordering of the crystal. Cracks, pores and channels may open up as the film undergoes widespread contraction of its out-of-plane lattice constant; these act as pathways for solvent molecules to move deeper into the film [*cf.* Fig. 6(b) and (c)], transforming more of the material into bulk phase and allowing the cracks to expand further. Even after the solvent is evacuated from the surface [*cf.* Fig. 6(d)], some residual solvent remains trapped within the cracks and pores due to capillary forces. Nevertheless, the solvent gradually evaporates over time ($\Delta\lambda_{min}$ continues to decrease), thus the remaining solvent exerts a capillary pull on the facets in the cracks, in an attempt to pull the crystallites back together and keep the surface energy low as internal surfaces become exposed. This brings the lamellar crystallites into an aligned position similar to the pre-annealing state, which scatters X-rays more coherently. Experimentally, this is seen as $(001)_{BS}$ becomes very intense [*cf.* (5) in Fig. 4(b)]. We believe that capillary pull leads to improved diffraction signal from the sample until enough of the solvent is removed, allowing the structure to relax to a semi-distorted state once more. This explanation is speculative and requires additional experimental validation and possibly computer simulations which are outside the scope of this article.

Conclusions

In summary, we have investigated the solvent vapor annealing process of a model thin film of pentacene by combining time-resolved optical reflectometry with time-resolved GIWAXS. The optical and X-ray measurements offer valuable insight into the solvent vapor annealing process. The optical measurements reveal that a substantial amount of acetone condenses at the surface of pentacene. Close inspection of optical and GIWAXS measurements shows no indication that the film dissolves or becomes structurally disordered, with the exception of a degradation of the lamellar structure. The onset of "thin film" to bulk phase transformation is observed upon exposure to solvent, and more bulk phase appears when the vapor pressure increases, indicating evidence for a solid–solid phase transition.

Time-resolved GIXD measurements allow us to observe an unusual transient behavior, whereby the total scattering power of the sample increases over a period of minutes, peaks, and then decrease once more. The unusual peaking behavior is believed to be due to a temporary realignment of crystallites as a result of capillary pull caused by evacuating residual solvent from pores and cracks formed in the thin film by the lattice contraction that accompanies phase change from the "thin film" to the bulk phase.

Acknowledgements

The authors would like to thank Dr Jim Elman from FilMetrics, Inc. for helpful discussions and the J. A. Woollam Co., Inc. for providing a copy of the WVASE32 software. This work was supported by the Cornell Center for Materials Research, a National Science Foundation Materials Research Science and Engineering Center (NSF DMR-0520404), and was performed in part at the Cornell High Energy Synchrotron Source, also supported by the National Science Foundation and NIH-NIGMS (NSF DMR-0225180). Part of this work was also performed at the Cornell NanoScale Facility, a member of the National Nanotechnology Infrastructure Network, which is supported by the National Science Foundation (Grant ECS 03-35765). One of us (V. P.) would like to acknowledge the National Science Foundation for a graduate fellowship.

Notes and references

1 C. D. Dimitrakopoulos and P. R. L. Malenfant, *Adv. Mater.*, 2002, **14**, 99–117.
2 Z. Bao, *Adv. Mater.*, 2000, **12**, 227–230.
3 C. J. Brabec, *Sol. Energy Mater. Sol. Cells*, 2004, **83**, 273–292.
4 L. Schmidt-Mende, A. Fechtenkötter, K. Müllen, E. Moons, R. H. Friend and J. D. Mackenzie, *Science*, 2001, **293**, 1119–1122.
5 G. Li, V. Shrotriya, J. Huang, Y. Yao, T. Moriarty, K. Emery and Y. Yang, *Nat. Mater.*, 2005, **4**, 864–868.
6 K. C. Dickey, J. E. Anthony and Y.-L. Loo, *Adv. Mater.*, 2006, **18**, 1721–1726.
7 Y. Kim, S. Cook, S. M. Tuladhar, S. A. Choulis, J. Nelson, J. R. Durrant, D. D. C. Bradley, M. Giles, I. McCulloch, C.-S. Ha and M. Ree, *Nat. Mater.*, 2006, **5**, 197–203.
8 D. Chirvase, J. Parisi, J. C. Hummelen and V. Dyakonov, *Nanotechnology*, 2004, **15**, 1317–1323.
9 S. Günes, H. Neugebauer and N. S. Sariciftci, *Chem. Rev.*, 2007, **107**, 1324–1338.
10 M. Campoy-Quiles, T. Ferenczi, T. Agostinelly, P. G. Etchegoin, Y. Kim, T. D. Anthopoulos, P. N. Stavrinou, D. D. C. Bradley and J. Nelson, *Nat. Mater.*, 2008, **7**, 158–164.
11 J. H. Park, J. S. Kim, J. H. Lee, W. H. Lee and K. Cho, *J. Phys. Chem. C*, 2009, **113**, 17579–17584.
12 D. Knipp, R. A. Street, A. Völkel and J. Ho, *J. Appl. Phys.*, 2003, **93**, 347–355.
13 S. Jung, T. Ji and V. K. Varadan, *Appl. Phys. Lett.*, 2007, **90**, 062105.
14 R. J. Chesterfield, J. C. McKeen, C. R. Newman, P. C. Ewbank, D. A. da Silva Filho, J. L. Bredas, L. L. Miller, K. R. Mann and C. D. Frisbie, *J. Phys. Chem. B*, 2004, **108**, 19281–19292.
15 D. Guo, S. Ikeda, K. Saiki, H. Miyazoe and K. Terashima, *J. Appl. Phys.*, 2006, **99**, 094502.
16 G. Beernink, T. Strunsukus, G. Witte and Ch. Wöll, *Appl. Phys. Lett.*, 2004, **85**, 398–401.
17 A. Amassian, V. A. Pozdin, T. V. Desai, S. Hong, A. R. Woll, J. D. Ferguson, J. D. Brock, G. G. Malliaras and J. R. Engstrom, *J. Mater. Chem.*, 2009, **19**, 5580–5592.
18 S. A. Burke, J. M. Topple and P. Grütter, *J. Phys.: Condens. Matter*, 2009, **21**, 423101.
19 D. Käfer, C. Wöll and G. Witte, *Appl. Phys. A: Mater. Sci. Process.*, 2009, **95**, 273–284.
20 T. Ji, S. Jung and V. K. Varadan, *Org. Electron.*, 2008, **9**, 895–898.
21 M. Fujihira, L.-M. Do, A. Koike and E.-M. Han, *Appl. Phys. Lett.*, 1996, **68**, 1787–1790.

22 Y. Qiu, Y. C. Hu, G. F. Dong, L. D. Wang, J. F. Xie and Y. N. Ma, *Appl. Phys. Lett.*, 2002, **81**, 4643–4646.
23 A. Maliakal, K. Raghavachari, H. Katz, E. Chandross and T. Siegrist, *Chem. Mater.*, 2004, **16**, 4980–4986.
24 Z. T. Zhu, J. T. Mason, R. Dieckmann and G. G. Malliaras, *Appl. Phys. Lett.*, 2002, **81**, 4643–4646.
25 H. Yang, L. Yang, M.-M. Ling, S. Lastella, D. D. Gandhi, G. Ramanath, Z. Bao and C. Y. Ryu, *J. Phys. Chem. C*, 2008, **112**, 16161–16165.
26 G. Yoshikawa, J. T. Sadowski, A. Al-Mahboob, Y. Fujikawa, T. Sakurai, Y. Tsuruma, S. Ikeda and K. Saiki, *Appl. Phys. Lett.*, 2007, **90**, 251906.
27 S. J. Gregg and K. S. W. Sing, *Adsorption, Surface Area and Porosity*, 2nd edition, Academic Press, London, 1982.
28 O. Hagemann, M. Bjerring, N. Chr. Nielsen and F. C. Krebs, *Sol. Energy Mater. Sol. Cells*, 2008, **92**, 1327–1335.
29 J. A. DeFranco, B. S. Schmidt, M. Lipson and G. G. Malliaras, *Org. Electron.*, 2006, **7**, 22–28.
30 J. K. Lee, P. G. Taylor, A. A. Zakhidov, H. H. Fong, H. S. Hwang, M. Chatzichristidi, G. G. Malliaras and C. K. Ober, *J. Photopolym. Sci. Technol.*, 2009, **22**, 565–569.
31 D. J. Gundlach, T. N. Jackson, D. G. Schlom and S. F. Nelson, *Appl. Phys. Lett.*, 1999, **74**, 3302–3304.
32 H. Yoshida and N. Sato, *Appl. Phys. Lett.*, 2006, **89**, 101919.
33 S. Miller, G. Fanchini, Y.-Y. Lin, C. Li, C.-W. Chen, W.-F. Su and M. Chhowalla, *J. Mater. Chem.*, 2008, **18**, 306–312.
34 K. C. Dickey, J. E. Anthony and Y.-L. Loo, *Adv. Mater.*, 2006, **18**, 1721–1726.
35 W. H. Lee, D. H. Kim, J. H. Cho, Y. Jang, J. A. Lim, D. Kwak and L. Cho, *Appl. Phys. Lett.*, 2007, **91**, 092105.
36 D.-M. Smilgies, P. Busch, D. Posselt and Christine M. Papadakis, *Synchrotron Radiat. News*, 2002, **15**, 35–41.
37 D.-M. Smilgies, R. Li, Z. Di, C. Drako, C. M. Papadakis and D. Posselt, *Mater. Res. Soc. Symp. Proc.*, 2009, **1147**, OO01-01.
38 U. Heinemeyer, R. Scholz, L. Gisslén, M. I. Alonso, J. O. Ossó, M. Garriga, A. Hinderhofer, M. Kytka, S. Kowarik, A. Gerlach and F. Schreiber, *Phys. Rev. B: Condens. Matter Mater. Phys.*, 2008, **78**, 085210.
39 A. Hinderhofer, U. Heinemeyer, A. Gerlach, S. Kowarik, R. M. Jacos, Y. Sakamoto, T. Suzuki and F. Schreiber, *J. Chem. Phys.*, 2007, **127**, 194705.
40 J. Chen, C. K. Tee, J. Yang, C. Shaw, M. Stein, J. Anthony and D. C. Martin, *J. Polym. Sci., Part B: Polym. Phys.*, 2006, **44**, 3631–3641.
41 E. J. Kintzel, Jr., D.-M. Smilgies, J. G. Skofronick, S. A. Safron and D. H. Van Winkle, *J. Vac. Sci. Technol., A*, 2004, **22**, 107–110.
42 A. C. Mayer, A. Kazimirov and G. G. Malliaras, *Phys. Rev. Lett.*, 2006, **97**, 105503.